

# Embedding Ionic Hydrogel in 3D Printed Human-Centric Devices for Mechanical Sensing

Baanu Payandehjoo, Tsz Ho Kwok\*

*<sup>a</sup>Department of Mechanical, Industrial and Aerospace Engineering, Concordia University, Canada*

---

## Abstract

Flexible sensor applications have increasingly focused on ionically conductive hydrogels due to their notable deformability and easily tunable properties compared to rigid materials. These hydrogels possess electrical properties, thanks to their high water content and porous structure that facilitate effective ion transfer. Despite their attractive features, hydrogels have limitations in terms of water retention and shape fidelity, and they are more typically inspected as two dimensional films and patches. In this paper, 3D printed thermoplastic polyurethane (TPU) elastomer frames with various geometries were injected with ionic conductive polyacrylamide (PAAm) based hydrogels to create durable, robust soft mechanical sensors for detecting strain, pressure, and bending through changes in their electrical resistance. After the effectiveness of the TPU encasement in maintaining the hydrogel water content was demonstrated, hydrogel embedded frames with varying geometries were designed. Their response to mechanical loading was investigated in relation to their dimensions and geometric shape. Finally, glove-shaped frames were fabricated to fit human fingers and injected with ionic hydrogel for sensing abilities. The wearable sensors accommodated free movement of the fingers in multiple directions and were able to detect simultaneous and independent bending and stretching of the fingers. Through comprehensive observation of the electrical behavior of all soft ionic sensors in response to different kinds of mechanical stimuli, it was concluded that the resistance change following mechanical loading was dependent on the specific geometric features of each individual hybrid sensor. Thus, ionic hydrogel-embedded TPU encasement could be designed with targeted geometry to dictate the type and direction of mechanical sensing with regard to its application. This work presents a facile approach to fabricating multi-component soft geometric sensors with potential to be used for wearable electronics and human-machine interactions.

*Keywords:* Ionic hydrogel, Mechanical sensing, 3D printing, Human-centric, Sensor.

---

## 1. Introduction

Flexible electronics have been gaining increasing attention among researchers following the advancement of human-machine interactions in a myriad of areas, such as soft robotics, wearable electronics, and personal healthcare monitoring [1, 2, 3]. Although rigid materials are more deeply understood and have better electrical performance, flexible components can better accommodate large, repeated deformations and conform to non-conventional surfaces. The expanding pool of information on flexible stimuli-responsive devices has shown their potential in fields where stretchability, transparency, and biocompatibility are key, while rigid electronics struggle to comply [4]. Hydrogels—one of the most workable examples of these soft materials—are three-dimensional (3D) polymer networks that contain water within their structure. Their hydrophilic behavior enables the absorption of ionic solutions and water by the free volume between the polymer chains, which endow conductivity through ion migration. Because of their significant water content and porous structure, ionic hydrogels can undergo large deformations under mechanical stimuli, such as strain, pressure, bending, and even smaller forces, like vibration. Changes in the material dimensions alter pathways through which the ions move, correspondingly changing its conductance and supplying

it with sensing abilities [5, 6, 7]. Regarding the performance of hydrogel ionotronics, the steps to fabricate the devices are as central as the electronics portion of the process. Changing the main and auxiliary constituents of the polymer solution and polymerization parameters can help control some characteristics of the final hydrogel product, which grants them a significant advantage in the tunability of their performance [8]. 3D printing can also fabricate hydrogels with various geometries [9], from an octet truss [10] to heart valves and other anatomical structures for medical devices [11].

Although hydrogels have many attractive features and can be 3D printed, they are still usually inspected as two-dimensional components like skin-like films and patches [12], and they are mostly used underwater or in vivo. This is because they have low shape fidelity and lose water quickly. While their aqueous nature results in favorable ductility and permeability, they simultaneously bound their ability to hold stable, irregular shapes, especially on larger scales [13]. In addition, the high surface-area-to-volume ratio of a complex shape increases the rate of water evaporation from the hydrogels when they expose to the ambient environment. The water content is the primary means of ion transport inside the porous structure and correlates directly with its conductive properties. Finding a proper balance in hydrogels can be a laborious task. Their deformability, strength, conductivity, and water retention are all highly interdependent, and changing one factor in the fabrication pro-

---

\*Corresponding author. Email: tszho.kwok@concordia.ca

cess can compromise others entirely. For example, adding a printability parameter to the selection of hydrogels puts heavier constraints on the qualified monomers and their desired functionalities [9]. Some research adds hydratable salts to the hydrogel to help keep the water content [14]. However, this way can only slow down the evaporation a bit, the hydrogel still dries up, eventually. With the growing interest in flexible electronics and personalized functional products, there is a need to make hydrogels long-lasting in ambient working conditions.

The traditional way of fabricating hydrogels is molding, where the hydrogel is injected into and solidified in a mold [15, 16]. The mold is unwanted and will be peeled off to release the hydrogel. However, we have an observation that electronics are seldom alone. For example, a printed circuit board is encased in a shell to make a functional mouse. Instead of creating a mold just to shape the hydrogel, we propose to design the mold as part of the device and to function together with the hydrogel. In this way, the mold can protect the hydrogel from water loss and also provide support for the hydrogel to have a higher shape complexity. The research questions here are how effective in water retention this encapsulation is, and how it affects the hydrogel's sensibility. The objective of this paper is to test this proposed method and answer the above questions. Specifically, a hybrid hydrogel-elastomer strain sensor is developed. Through 3D printing, we fabricate custom hollow frames with various geometries using thermoplastic polyurethane (TPU). Photopolymerizable ionic hydrogel solution is then injected into the frame structures and UV-cured to get the final conductive elastomer. Afterward, the soft conductors are used as sensors, which transduce mechanical stimuli into electrical signals to identify strain, pressure, and bending. The contributions of this work are

- We present a novel production method for flexible electronics by 3D printing hollow elastomer frames to encase ionic hydrogels and function together.
- We test and confirm that this fabricated hydrogel has higher durability and enhanced water retention abilities.
- We design various geometries for the hydrogel-based devices to show that they are sensitive enough to give diverse responses to different motions.

The experimental results show the potential of this hydrogel-embedded complex elastomer geometries to be used in wearable electronics and human-machine interactions.

The rest of the paper is organized as follows. In Section 2, related works will be presented. Section 3 will outline the preparation and characterization steps of the materials. Evaluation of samples and the methodology leading to custom-designed stretchable conductors will be discussed in Section 4. Finally, Section 5 includes analysis and discussion of experimental results, followed by a conclusion in Section 6.

## 2. Related Works

In 2014, Sun et al. [17] presented a type of artificial skin in the form of ion-charged hydrogel structures called Ionic

Skin (or I-Skin) by adding sodium chloride to their composition. Ever since, many have reported using different types of salt to provide hydrogels with electrical conductivity. Additionally, due to the strong interactions of ions with water molecules through the ion solvation effect, adding salt to the hydrogel composition enhances their water retention abilities, which directly correlates to their mechanical and electrical behavior [18]. Besides providing hydrogels with ionic conductivity, hygroscopic salts have been shown to reduce vapor pressure and slow down moisture evaporation by creating additional crosslinks and reducing pore size within the polymer structure. These extra crosslinks can also act as dynamic "sacrificial bonds", contributing to the strength and toughness of the hydrogel [19]. Although it is a simple and effective way to enhance their durability, their behavior remains highly dependent upon environmental conditions, and most of them still face barriers in practical long-term applications [20, 21]. Sui et al. [22] used LiCl to fabricate an ionic conductive hydrogel with the ability to retain its water content after a week in ambient conditions. Multivalent salts such as  $\text{FeCl}_3$  have been used for higher conductivity due to the higher number of free ions they release, as well as restricting water evaporation by increasing crosslinks in the hydrogel structure which causes smaller pores where charge passes through [23]. Other than salts, the incorporation of chitosan chains into hydrogel compositions has also been explored to enhance the strength and toughness of the gels. By introducing chitosan, non-covalent bond interactions are formed which enhance the strength and toughness of the structure, as described by Ahmadi et al. [24]. The inclusion of this biopolymer in the hydrogel solution leads to an increase in crosslink density of the polymer network, resulting in a higher viscosity of the solution.

Another approach to minimizing water loss from hydrogel surfaces is covering them with a VHB tape [25]. Adding a hydrophobic polymer coating to the hydrogels creates a barrier against water evaporation and helps keep hydrogel properties steady and long-lasting. Hydrophobic silicone-based coatings like polydimethylsiloxane (PDMS) and (3-aminopropyl) triethoxysilane (APTES) are examples of polymers used to shield the hydrogel surface from external environments for days. Controlling the stability of such an instrumental quality of hydrogels dictates the service life of soft sensors based on these aqueous entities [26, 27].

Additive manufacturing has been adopted for producing both pure hydrogels and polymer-hydrogel hybrid devices with more versatile, geometrically complex structures [28], but not all kinds of hydrogel compositions meet the standard qualifications demanded by the particular working mechanisms of commercial 3D printers. Throughout the years, the required properties for printability of soft materials have been obtained by adding auxiliary components, e.g. nanoclay [29], nanocellulose [30], and graphene oxide [31] to thicken gel solutions, combining multiple hydrogels to improve mechanical properties [32], controlling printing temperature [33] and engineering custom printer heads that are capable of printing under particular conditions [11]. Some have employed a two-step crosslinking method in which the hydrogel solution first undergoes phys-

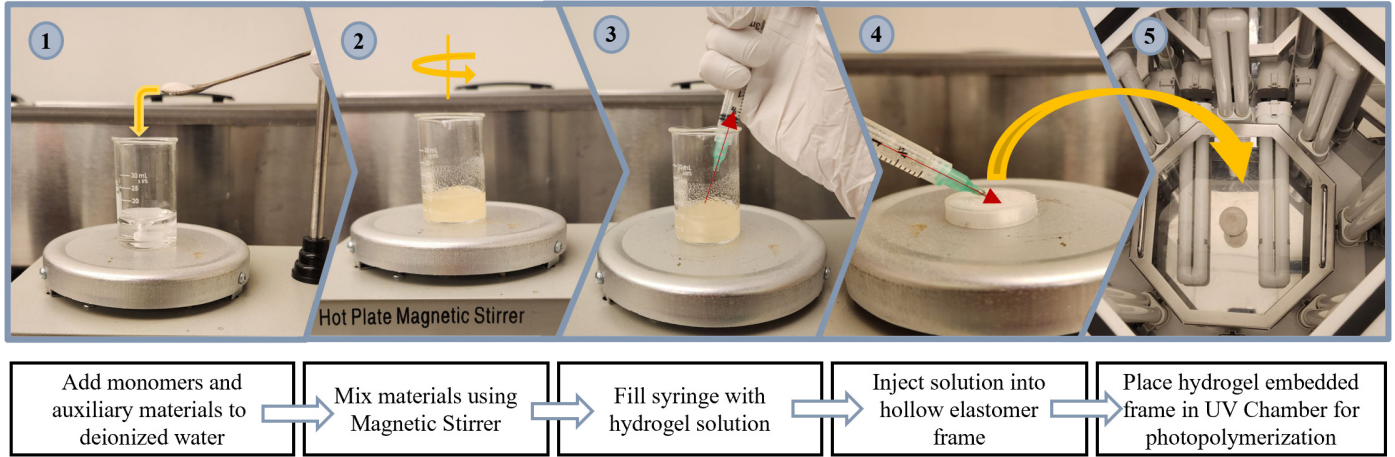


Figure 1: Fabrication steps of the ionic hydrogel embedded 3D printed elastomer sensor

ical crosslinking before the 3D printing process, and is then photo-crosslinked as a post-treatment to enhance print quality and shape fidelity [34].

Dynamic hydrogel circuits have been fabricated on a millimeter scale using projection microstereolithography ( $P\mu$ SL) which can be locally degraded and repaired to modify the circuit configurations for multiple functional human interfaces [35]. For hybrid stretchable materials, a recurring method has been to alternatively switch between two precursors to print combinations of hydrogels and different polymers toward the development of more efficient and feasible gel-based electronic devices [28, 36]. Although all aforementioned research shows vast development in the design and fabrication of three-dimensional hydrogels, a simple method to manufacture geometrically complex hydrogel-based devices regardless of their chemistry and composition is yet to be presented.

### 3. Materials and Methods

#### 3.1. Materials

All the chemicals were used as received without further purification. Acrylamide (AM), Acrylic Acid (AA), N,N-methylene-bisacrylamide (MBA), Iron (III) Chloride ( $FeCl_3$ ), 2-hydroxy-4'-(2-hydroxyethoxy)-2-methylpropiophenone (Irgacure 2959), short-chain chitosan (degree of deacetylation > 75-85%, viscosity 20-300 mPa s for 1% (w/v) in 1% acetic acid solution, and molecular weight = 50-190 kDa) were purchased from Sigma-Aldrich (St. Louis, Missouri, USA). Sodium Chloride (NaCl), i.e., table salt, was purchased from local stores. 1.75 mm water translucent CHEETAH TPU filament was purchased from NinjaTek (Manheim, Pennsylvania, USA).

#### 3.2. Equipment

The equipment used for the fabrication of the samples and devices includes a magnetic stirrer from INTLLAB (Greenwood, Indiana, USA), an Ultrasonic Cleaner from Canada Ultrasonics (Newmarket, Ontario, Canada), a Comgrow Creality 3D Ender 5 3D Printer from Creality3D (Shenzhen, China),

an LC-3DPrint Box UV Post-Curing Unit from NextDent (Soesterberg, The Netherlands), a PM18C True RMS Multifunctional Digital Multimeter from Aidbucks (China) and an Arduino Uno Rev3 from Arduino. All chemical silverware and glassware were purchased from Sigma-Aldrich (St. Louis, Missouri, USA).

#### 3.3. Fabrication

The fabrication process of the hybrid sensor is shown in Fig. 1. The hydrogel was synthesized by firstly mixing AM (2.2 g), MBA (0.03 mol%) as the crosslinking agent, Irgacure 2959 (54.0 mg) as the photoinitiator, NaCl as an electrolyte, and short-chained chitosan (CS) in 10 mL of deionized water, and then gradually adding AA (15% molar ratio of AA/AM) to prevent a sudden increase in viscosity and difficulty in stirring (Steps 1 and 2). The concentrations of monomers, crosslinker, and photoinitiator were taken from Liu et al. [19]. The solution was degassed at 50°C for 3 to 5 minutes in an ultrasonic cleaner, depending on the viscosity of the liquid. To fabricate the bare samples, the solution was then poured into molds and cured under UV light (18 W, 365 nm) in an LC-3DPrint Box.

The hollow elastomer frames were designed in Fusion 360 software. TPU filament was used to realize the designs using a Creality Ender 5 3D printer. Additive manufacturing was done at 35 mm/s print speed, 0.1 mm print accuracy, and a temperature of 235°C. After the object was printed, the prepared pre-cure gel solution was gathered into a syringe (Step 3) and injected into the hollow elastomer frame (Step 4). After the hybrid samples were irradiated under UV light (Step 5), they were connected to an Arduino Uno setup to be tested for mechanical sensing.

#### 3.4. Characterization

##### 3.4.1. Water Retention

The water retention ability of bare and encased hydrogels with various compositions was assessed by repeatedly recording their weight at different times. The change in water content

was reported in terms of the percentage of weight lost:

$$\Delta W = \frac{W_0 - W}{W_0} \times 100, \quad (1)$$

where  $W$  is the weight of the sample at different times, and  $W_0$  is the weight at  $t = 0$ .

### 3.4.2. Mechanical Sensing

The electrical resistance of any material follows Pouillet's law of resistivity:

$$R = \rho \frac{l}{A}, \quad (2)$$

where  $\rho$  is the material resistivity,  $l$  is the sample length, and  $A$  its cross-section, indicating that the resistance of an object is dependent on its dimensions, and thus directly affected by deformation.

To assess the dependence of their electrical properties on mechanical stimuli, the change in resistance of the ionic hydrogels was observed and calculated by

$$\Delta R = \frac{R - R_0}{R_0} \times 100, \quad (3)$$

where  $R$  is the resistance at each moment, and  $R_0$  is the initial resistance of the sample. To measure resistance change under different amounts of mechanical loading, an Arduino Uno ohmmeter was used. The response of the ionic hydrogel to strain, pressure and bending was tested.

## 4. Results

To test for water retention properties and mechanosensitivity, acrylamide-based hydrogels were fabricated with fixed concentrations of auxiliary materials, which were adjusted as necessary to achieve desired properties. As a hydrophilic polymer, polyacrylamide has good water absorption, but relatively low hydrolytic stability and mechanical properties. The copolymerization of acrylamide with acrylic acid confers ion exchange properties on the hydrogel as well as increasing its water retention ability and tensile strength. Additionally, crosslinking the copolymer with MBA through a vinyl addition polymerization results in a gel with varying porosities depending on the concentration of the crosslinker and monomers, and polymerization conditions [37]. To examine the impact of chitosan, various hydrogel samples were created with varying amounts of the substance. The samples were then tested to determine how chitosan affected their injectibility into elastomer frames and water retention behavior in both bare and TPU-encased hydrogels. The ionic hydrogels demonstrated satisfactory mechanosensitivity, and hybrid elastomer/hydrogel designs were shown to display distinguishable signals under different types of mechanical stimuli.

Table 1: Composition of Hydrogel Samples

Sample	Chitosan	TPU
PAAm	×	×
200-CS-PAAm	200mg	×
450-CS-PAAm	450mg	×
700-CS-PAAm	700g	×
Hybrid	×	YES
450-CS-Hybrid	450mg	YES

### 4.1. Comparing the Rate of Water Loss

As shown in Table 1, four polyacrylamide (PAAm) based samples were generated, three of which contained different amounts of chitosan (CS) (labeled 200-CS-PAAm, 450-CS-PAAm, and 700-CS-PAAm). The Hybrid and 450-CS-Hybrid samples consisted of hydrogel-embedded round TPU frames. After fabrication, all the samples were left to air dry in the same ambient conditions for up to 60 hours to compare their water retention ability and durability.

Initial water content was calculated to be approximately 80 w% for all bare and encased samples based on the ratio of deionized water to the total materials used to prepare the pre-cure polymer solution. It is seen in Fig. 2c that chitosan content contributes to maintaining water within the polymer chains of the ionic hydrogel. This effect is due to the extra crosslinks that the chitosan molecules create with the main polymer chains consisting of PAAm and AA. With an increase in the number of crosslinks within the hydrogel structure, the free volume formed between the polymer chain is divided into smaller sections. Following the decrease in the pore size, water molecules are better entrapped within the chains, which hinders their evaporation from the polymer structure. Accordingly, the results of the water retention tests displayed in Fig. 2c show chitosan content had a positive effect on the water retention ability of the hydrogels, although small. While 60% of the PAAm samples initial water content evaporated in under 15 hours, 700-CS-PAAm lost 54%, on average. Within 60 hours, the results remained consistent as PAAm, 200-CS-PAAm, 450-CS-PAAm and 700-CS-PAAm lost 85.5%, 84.8%, 81.8% and 78.2% of their water, respectively. After losing most of their water content, the samples no longer maintained their gel-related behavior and acted as brittle non-aqueous polymers. Considering the minimal contribution of chitosan to the water retention abilities of the hydrogels, this rate of water loss within a small time frame necessitated a different approach to ensure the durability of the hydrogel's mechanical and electrical behavior. This issue was addressed by the fabrication of elastomer encasements for the hydrogels through extrusion 3D printing.

Hollow TPU frames were fabricated to fully cover the hydrogels and protect them from the external environment, and further improve their water retention. To evaluate the efficacy of this method, cylindrical TPU disks (illustrated in Fig. 2b) were fabricated to mimic the exact shape and dimensions of the polymerized bare hydrogels (Fig. 2a). The frames were injected with pre-cure hydrogel solution which was then solidified under UV irradiation. It is clearly observed in Fig. 2d that

the protective encasements were highly effective in obstructing water evaporation from the hydrogel surface. While 80% of the water content of PAAm and 450-CS-PAAm evaporated after 30 hours, the Hybrid and 450-CS-Hybrid samples lost only 1.9% and 1.3% after 60 hours, respectively. Although chitosan content in both hybrid samples seemed insignificant in the matter of water retention, it contributed in terms of injectibility and compatibility with the elastomer surface. The more viscose 450-CS-PAAm was injected into the frame more conveniently, spreading out uniformly into the empty space without forming any air bubbles. After polymerization, even though both encased hydrogels showed higher durability in water related properties, 450-CS-Hybrid exhibited more structural stability as the hydrogel from the Hybrid sample dislodged from the inner TPU layer and left air cavities inside the printed cylinder within 24 hours. This is possibly due to a larger mismatch between the hydrogel and TPU polymer in the Hybrid sample compared to 450-CS-Hybrid. The chitosan content increased the number of crosslinks within the polymer chains resulting in higher toughness and Modulus of the hydrogel, which brought it closer to the mechanical properties of the TPU elastomer frame. The dislodged location and area could vary case by case, and unpredictably compromise the structural and electrical behavior of the sample. Based on these results, 450-CS-Hybrid was chosen to be used in the following experiments regarding the complex geometry hybrid sensors.

#### 4.2. Bare Ionic Hydrogel

To set up a baseline, bare ionic hydrogels were fabricated to be evaluated for sensitivity to mechanical loading. The tests were done immediately after the samples were cured to eliminate the effects of water loss on sensitivity as much as possible.

Figure 3a demonstrates the response of two ionic hydrogel samples with different NaCl concentrations to static pressure. The signals had oscillations within the plateau but were easily distinguishable from when the hydrogels were left untouched. These oscillations may have been due to variations in static pressure, or unintended movements of the metal electrodes. The drop in overall resistance could be because when the external source of pressure was removed from the ionic hydrogel, the residual stress formed in the hydrogels during fabrication was released. This phenomenon led to the continual movement of the polymer chains with respect to each other, which changed the paths that permit ion transfer. The sample containing 2M NaCl was then used to test if the hydrogel would be able to discern different amounts of pressure. It can be observed from Fig. 3b that the resistance of the conductive hydrogel initially decreased by 29% when pressed lightly, and 43% when pressed heavily. This difference in responsivity implies that the electrical resistance of the hydrogel was sensitive to the extent of deformation. The more the hydrogel structure deformed and caused variations in ion migration paths, the more vastly its ionic conductance was altered.

#### 4.3. Hydrogel Embedded TPU Sensors

3D printing brings forth the possibility of creating ionic hydrogel sensors in various shapes and sizes, in contrast to their

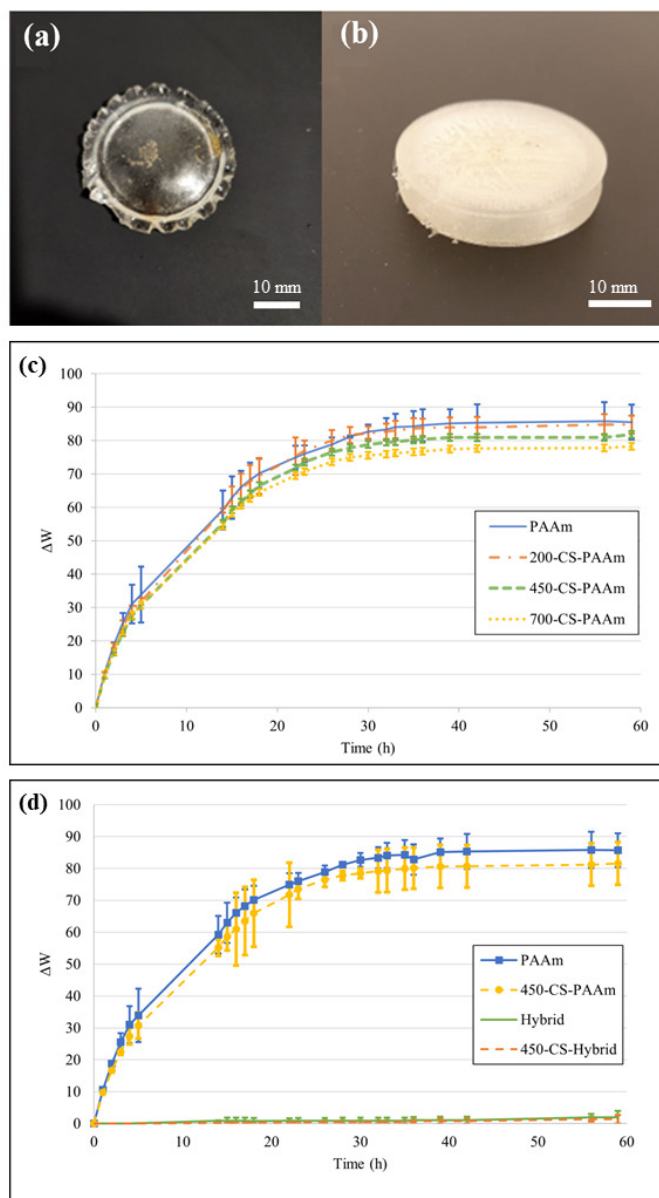


Figure 2: (a) Bare ionic hydrogel and (b) hydrogel embedded TPU frame for evaluation of water retention and material compatibility (c) Water loss (w%) of hydrogel samples with different chitosan content during 24 hours (d) Comparison of water loss (w%) in bare and encased hydrogels with and without chitosan content

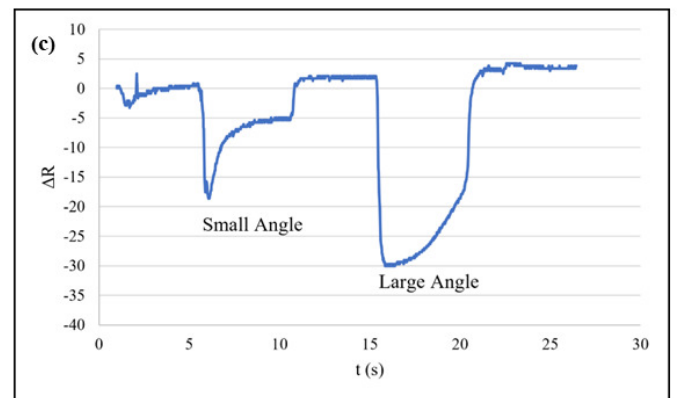
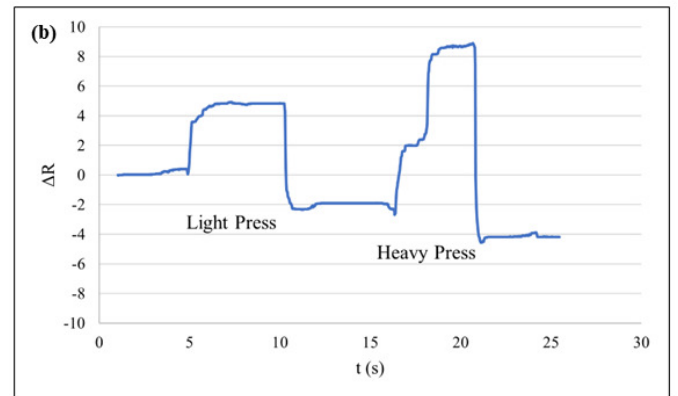
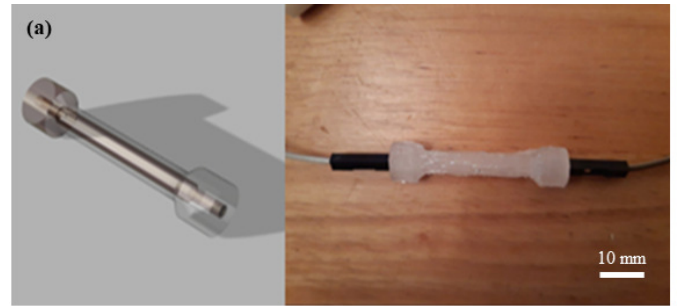
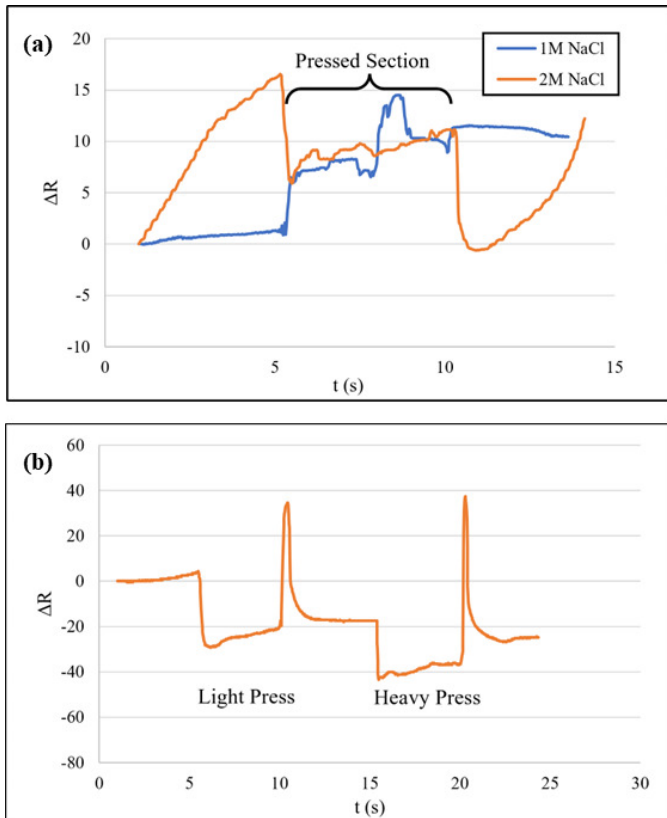


Figure 3: (a) Response of bare 1M-Na-PAAm and 2M-Na-PAAm samples to pressure (b) Response of bare 2M-Na-PAAm samples to light and heavy pressing.

more common thin-film form. After demonstrating the electrical sensitivity of bare ionic hydrogels to mechanical loading, 450-CS-PAAm samples containing 2M NaCl were injected into 3D printed TPU frames for higher geometric complexity, better water retention, and to eventually be able to control the direction of hydrogel deformation for mechanical sensing. Basic hybrid sensors were designed and printed for examining the response of the hybrid elastomer/hydrogel sensors to pressing, pulling, and bending based on the type of deformation that their designed geometry allowed. These geometries included a dogbone, a strain gauge, and a finger-shaped cylinder.

#### 4.3.1. Dogbone

The small dogbone object was designed with a cylindrical cavity to hold the hydrogel as shown in Fig. 4a. After curing, its response to pressing and bending was observed by inserting electrodes into its sides. It is demonstrated in Fig. 4b that the hybrid dogbone sensor responded with distinguishable signals when it was pressed lightly ( $\sim 0.5$  N) and heavily ( $\sim 1$  N) in the middle. The light press elicited a smaller increase in the resistance, up to 7.4%, while the heavy press caused an up to 8.6% increase in resistance. Additionally, Fig. 4c shows that bending the sensor at small and large angles was followed by resistance change corresponding to the bending angle. The section for large-angle bending shows a curve before returning to initial resistance which can be due to the gradual relaxation of

Figure 4: (a) CAD design and printed dogbone sensor (b) response of the dogbone sensor to light and heavy pressure and (c) small and large bending angles about its length.

the hybrid dogbone to its original shape. Some random signal peaks and inconsistencies also seen in the plots were attributed to the movement of the electrodes within the soft sensor.

#### 4.3.2. Strain Gauge

The strain gauge shown in Fig. 5a was injected with ionic hydrogel and evaluated for a response when pulled from both sides. In contrast to the dogbone, electrodes were inserted into the strain gauge pre-cure so that they would be entirely covered by the hydrogel after polymerization to diminish irrelevant signals. The strain gauge design in Fig. 5a was tested for response to mechanical loading by pulling the object from both sides. Figures 5b and 5c show the response of the hybrid sensor on two different data acquisition platforms in terms of resistance change. In Fig. 5b, small rises in resistance are observed in response to three consecutive cycles of pulling, which is due

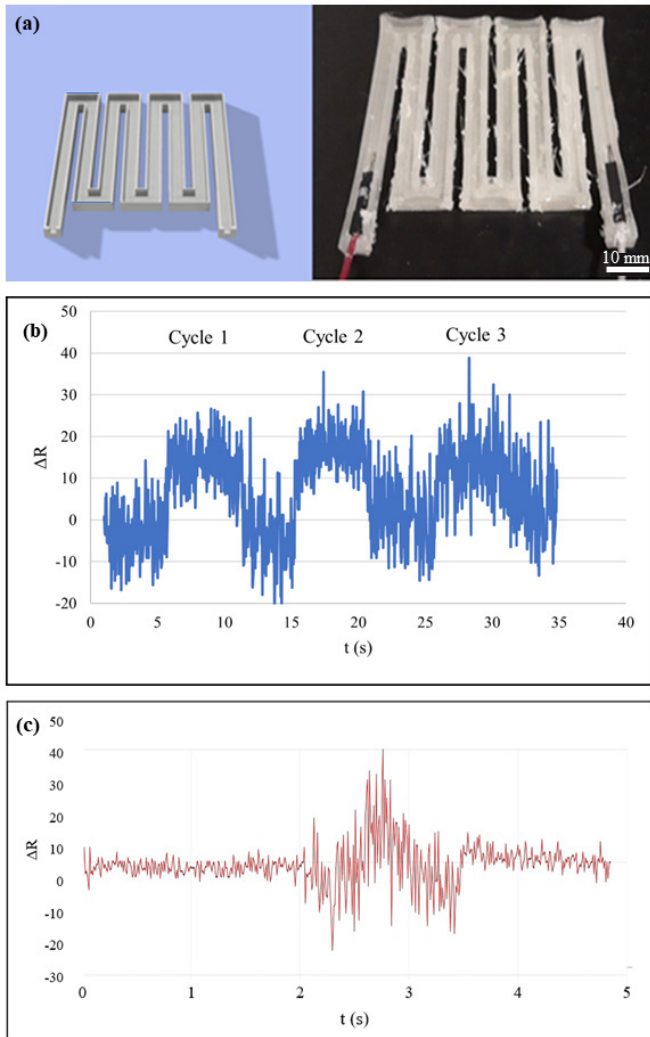


Figure 5: (a) CAD design and printed strain gauge (b) response of the strain gauge sensor to being pulled from both sides from CSV data and (c) on the Arduino UNO serial plotter platform in real-time.

to the lengthening of the path through which the ions transfer. In Fig. 5c, although a clear change in resistance was not observed, bigger oscillations in the electrical signal were visible, suggesting an external mechanical force was imparted onto the hybrid sensor. The relatively small electrical response possibly occurred because the object design did not properly accommodate expansion parallel to the pulling direction, leaving little room for deformation.

#### 4.3.3. Finger-shaped Cylinder

The design and print of the finger-shaped cylinder are shown in Fig. 6a. The cylinder was designed with a U-shaped cavity to hold the hydrogel. Figure 6b shows that the finger-shaped sensor was able to detect pressure both in the middle, at the bottom, and at the tip. While the response to pressing the middle and the bottom of the cylinder was exhibited as drops in the resistance, pressing the tip led to a smaller and positive percentage of resistance change.

As the final basic hybrid design, a finger-shaped cylinder was

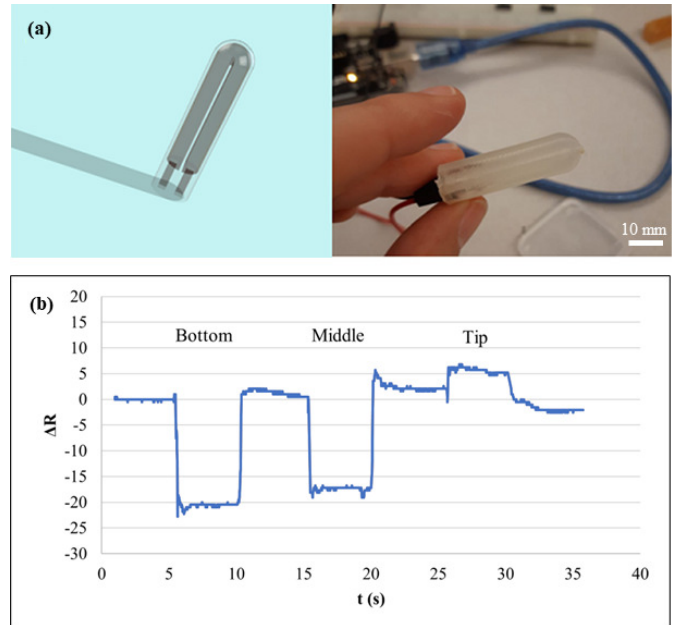


Figure 6: (a) CAD design and printed finger-shaped object (b) response of the finger-shaped sensor to being pressed in the middle, at the bottom, and the tip

designed with a U-shaped cavity to hold the hydrogel (Fig. 6a). For this sensor, two cubic spaces were also designed at the bottom where the electrodes would be inserted to fasten the electrodes in the device and reduce their movement for more precise responses to mechanical stimuli. The resistance change plot depicted in Fig. 6b shows that the sensor recognized pressure at different locations of the object. At the bottom and middle of the sensor, the resistance dropped around 20% and 16% respectively in response to pressure, indicating analogous sensitivity. In contrast, when the sensor was pressed at the tip, it increased by around 6%. This discrepancy could be attributed to the difference in hydrogel geometry within the particular design. While at the bottom and the middle, the hydrogel was deformed in two sections of its length, there was a continuous mass of hydrogel cured at the bottom of the “U” of the U-shaped cavity. This variation in geometry dictated the direction of deformation in the hydrogels following mechanical loading, which affected their electrical response at different locations.

#### 4.3.4. Glove-shaped Sensor 1

Subsequent to observing the response of the hybrid sensor to pressure, strain and bending, more complex objects were 3D printed to confine the ionic hydrogel. Firstly, a finger glove suited for three middle fingers of the human hand was printed, as shown in Fig. 7a. The design consisted of a main body to cover the fingers, and a bridge to connect them together to accommodate both bending and stretching apart.

As demonstrated in Fig. 7b, rises in the hydrogel resistance can be seen following three consecutive cycles of bending all three fingers simultaneously, which is ascribed to both the inward bending of the frame, and the outward pressure exerted onto the object from the back of the knuckles. Furthermore, the sensor also responded when the fingers were stretched apart

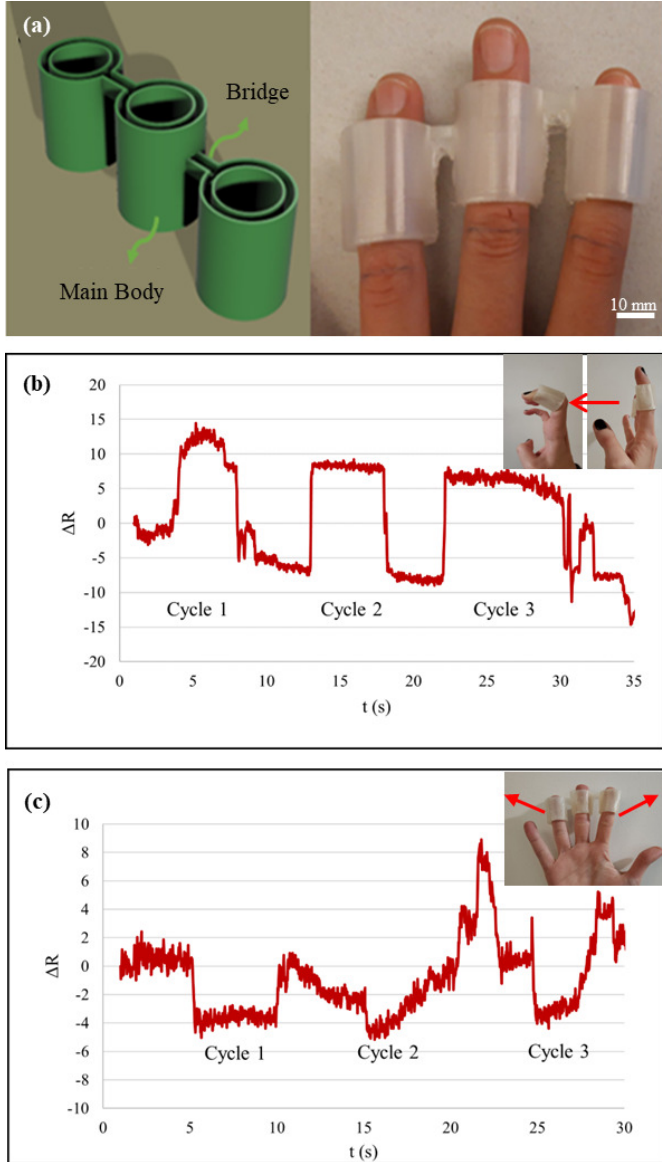


Figure 7: (a) CAD design and printed glove-shaped sensor 1, (b) its response to bending fingers and (c) stretching fingers apart for three cycles.

from each other by a decrease in resistance in three consecutive turns through the lengthening of the bridge components (Fig. 7c). Python code was used to detect and differentiate between bending the fingers and stretching them apart on the hybrid glove mechanical sensors. The pseudocode of the finger motion detection program can be seen in Algorithm 1.

Even though the hydrogel was able to respond well while confined in this geometry, the straight design of the bridges allowed for little extension, and the large surface area of the wearable sensor complicated the free and independent movement of the individual fingers. As a solution, a lighter, less constricting wearable sensor was designed, as shown in Fig. 8a.

#### 4.3.5. Glove-shaped Sensor 2

A lighter glove design with empty spaces in front of the knuckles was designed for more freedom of movement

#### Algorithm 1 Finger Motion Detection

```

1: Read the CSV file of the sensor response into Dataframe
2: Convert Dataframe to array 'data' with columns 't' and 'R'
3:  $bendSignal \leftarrow$  Bend Signal Threshold
4:  $tResponse \leftarrow$  40 iterations
5:  $pullSignal \leftarrow$  Pull Signal Threshold
6:  $pullEdge \leftarrow 1$  and  $bendEdge \leftarrow -1$ 
7:
8: for length of time series  $i$  do
9:    $deltaR \leftarrow data[i+tResponse][R] - data[i][R]$ 
10:
11:   if  $deltaR < pullSignal$  then
12:     if next iteration  $> pullSignal$  then
13:        $pullEdgeOld \leftarrow pullEdge$ 
14:        $pullEdge \leftarrow deltaR$ 
15:     if  $pullEdge \times pullEdgeOld < 0$  then
16:       Print 'Stretching at  $data[i][t]$ '
17:   if  $deltaR > -pullSignal$  then
18:     if next iteration  $< pullSignal$  then
19:        $pullEdgeOld \leftarrow pullEdge$ 
20:        $pullEdge \leftarrow deltaR$ 
21:     if  $pullEdge \times pullEdgeOld < 0$  then
22:       Print 'End of stretching at  $data[i][t]$ '
23:   if  $deltaR < bendSignal$  then
24:     if next iteration  $> bendSignal$  then
25:        $bendEdgeOld \leftarrow bendEdge$ 
26:        $bendEdge \leftarrow deltaR$ 
27:     if  $bendEdge \times bendEdgeOld < 0$  then
28:       Print 'Bending at  $data[i][t]$ '
29:   if  $deltaR > -bendSignal$  then
30:     if next iteration  $< bendSignal$  then
31:        $bendEdgeOld \leftarrow bendEdge$ 
32:        $bendEdge \leftarrow deltaR$ 
33:     if  $bendEdge \times bendEdgeOld < 0$  then
34:       Print 'End of bending at  $data[i][t]$ '

```

(Fig. 8a). The bridges which held the main body together were shaped into half moons to accommodate horizontal extension. This glove was also designed with space for the electrodes to be inserted into the pre-cure gel solution for better mechanical and electrical stability of the entire system. Figures 8b and 8c depict the response of the lighter glove-shaped sensor to stretching the Index and Middle fingers, and the Middle and Ring fingers in arbitrary units of resistance, respectively. Additionally, when the index, middle and ring fingers were bent down one by one, the wearable sensor responded with changes in its resistance, as shown in Figs. 8d, 8e, and 8f, respectively. The plots show significant drops in resistance as a result of bending the index and ring fingers, but smaller rises in resistance following the bending of the middle finger. This could be because the middle part of the glove was surrounded by two bridges and could hold less amount of conductive hydrogel in the empty space. Nevertheless, this design enabled relatively free and independent movement of all three fingers in more than one direction

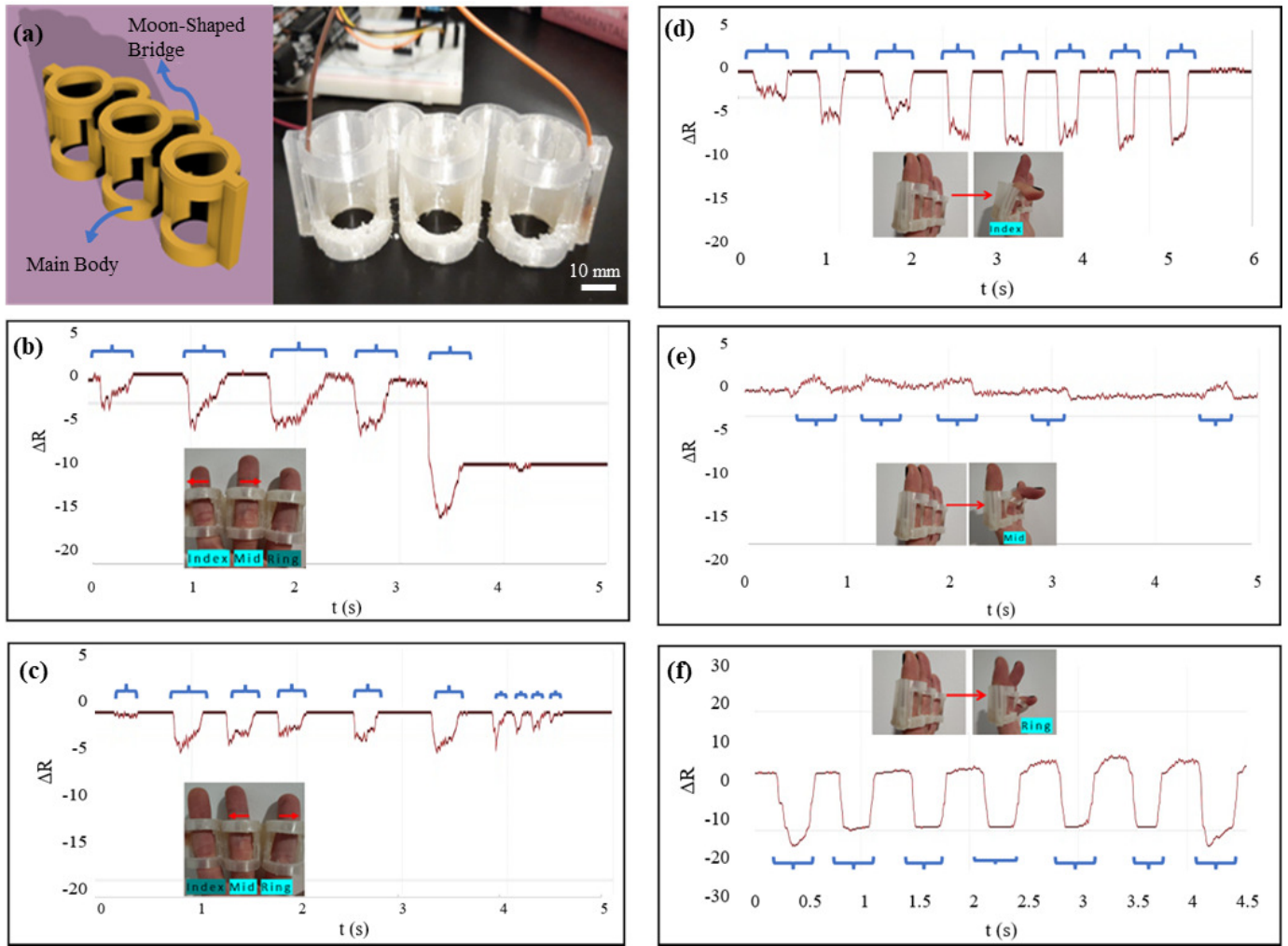


Figure 8: (a) CAD design and printed glove-shaped sensor 2 and its response to (b) stretching apart Index and Middle fingers, (c) stretching apart Middle and Ring fingers, (d) bending Index finger, (e) bending Middle finger, and (f) bending Ring finger. (Sections of the graphs that are marked with accolade symbols show the ranges in which the sensor was stimulated)

and was able to detect those movements through changes in the electrical signal.

## 5. Discussion

This research demonstrates that given the appropriate geometry, the hybrid hydrogel sensors responded to mechanical loading similarly to the bare ionic hydrogels, albeit with generally lower sensitivity due to the constriction of their deformability by the TPU elastomer. They also exhibited significantly lower rates of water evaporation than the bare hydrogels that were directly exposed to air, which faced issues in maintaining their electrical conductivity as well as their gel-related properties. The 3D printed TPU frames acted as encasements to cover the outer surface of the ionic hydrogels and protect them from water evaporation. Additionally, they enabled the design and fabrication of complex application-defined hollow geometries to counter the low mechanical stiffness of the aqueous hydrogel structure that diminishes their shape fidelity at larger scales. These hybrid objects could be designed in specific shapes to

accommodate the detection of mechanical stimuli in different forms and directions.

Comparing the results from electrical tests on the bare (Fig. 3) and encased ionic hydrogels (e.g., Fig. 5), it is clear that the bare hydrogels and the hybrid samples have similar sensitivity, i.e., they both have similar changes in resistance, around 10-40%. This means that although the lower flexibility of the TPU elastomer increases the elastic modulus of the hybrid system, it does not affect much the hydrogel performance. Also, there are sudden large peaks seen at the end of the response signal in the bare hydrogel after the pressure is removed from the sample. These peaks are caused by movements in the electrodes, changing their contact area with the conductive hydrogel. Conversely, there are no such peaks seen in the resistance change of the hybrid samples, where electrodes were fixed in solidified hydrogel and in-between robust elastomer walls.

We observe that the signals in the strain gauge sample in Fig. 5 have much more fluctuations than other examples. This should not blame the encasement, because the dogbone and cylinder samples also with encasement in Figs. 4 and 6 show

stable responses. The difference between them is the travel length of the ions. The S-shaped strain gauge has a much longer travel length, which results in more noise and instability. However, the change in resistance to mechanical stimuli is still prominent. Having sharp edges might also be a factor negatively affecting the smoothness of the signals. The appropriate length and cross-section of the glove designs in Figs. 7 and 8 allowed them to acquire detectable resistance change from the movement of fingers, following the same deductions. Therefore, the mechano-electrical properties of the hydrogel-based sensors were considerably influenced by various geometrical parameters in addition to their chemical composition.

In general, the complex geometry of the elastomer/hydrogel sensors made it difficult to analyze the reasons behind the patterns of resistance change, due to the multifarious parameters affecting the deformation and conductance of the hydrogels. Ultimately taking note of the response patterns in all of the diverse designs demonstrated for the hybrid ionic sensors, geometry certainly played a large role in dictating the type and direction of mechanical loading and the variation in electrical signals when the conductive component of the devices was deformed. For instance, the dogbone design did not permit high amounts of strain to be exerted onto it, but was easily pressed and bent to obtain a significant electrical response (Figs. 4b and 4c, respectively). In contrast, the thin zig-zag shape of the strain gauge was not suitable to sense bending or pressure but had a response to being pulled from both sides. The more complex glove-shaped sensors (Figs. 7 and 8) accommodated movement and sensing in two directions. While the bridge sections of the design responded to the fingers being stretched apart from each other, the main body of the glove was able to detect the bending of the fingers. The significance of sensor geometry can once again be observed in the response of the second glove-shaped sensor, where the plots in Fig. 8 demonstrate its ability to detect independent bending and stretching of the fingers due to the less constricting main body, and more deformable circular bridges.

Tactile perception is one of the main functions that help human beings to perceive the external environment. These durable, robust hybrid sensors can be employed as medical prosthetic devices, sensors for healthcare monitoring, and human-robot interactions. Specifically, the glove-shaped sensors could be used for monitoring in physical therapy and rehabilitation, be it as a wearable or a conductive prosthetic device. Their ability to detect hand gestures and independent finger movements creates opportunities to translate the signals into meaningful outputs, such as musical notes, interpreting sign language, or commands for remote control. The possibility to customize designs and print hollow frames in desired geometries grants vast potential for a wider range of alternative applications for these hybrid elastomer/hydrogel sensors.

## 6. Conclusion

A series of hybrid elastomer/hydrogel devices were demonstrated as ionic mechanical sensors. The electronic devices consisted of an ionic conductive hydrogel component that was in-

jected into various 3D printed geometries to provide the hydrogel with protection from the external environment and enable the fabrication of complex three-dimensional geometries. The injected hydrogels were then cured under UV irradiation. Then, the hybrid devices were tested under pressure, strain, and bending for mechanical sensing functionality. As a result of deformation in the hydrogel structure, these ionic sensors were able to detect different types of mechanical loading through changes in resistance correlating to the amount of force exerted onto them. Moreover, hybrid wearable sensors were also designed and 3D printed. The hydrogel-embedded gloves were able to detect when the fingers were bent and stretched apart from each other. While taking into consideration the significance of hydrogel deformation and water retention, this paper shows that hollow frames can be designed in various shapes to encase hydrogels to fit a range of specific applications in human-machine interfaces, soft robotics, and personal healthcare monitoring.

The hybrid sensing system presented in this paper showed promise as a stretchable ionic sensor responding to different mechanical stimuli. Nevertheless, there is much room for improvement in its fabrication steps and operation. The relatively low sensitivity of the hybrid device due to its high resistance could be enhanced using stronger salts as the electrolyte and more suitable geometry designs for the body and cavities of the elastomer frame. Although the high durability of the hydrogel-embedded elastomers was demonstrated in terms of high water retention, cyclic stability of electrical properties and signal consistency could also be examined in the future. Furthermore, investigating the exact correlation between different geometrical features of the design and the electrical response could be useful in figuring out the best approaches to designing the 3D printed sensor for amplified response to mechanical loading. Elastomer filaments with varying elastic moduli can be used as hydrogel encasements to reduce the mismatch between elastomer and hydrogel mechanical properties. The effect of different elastomer frames on the hybrid sensor performance and workability could also be examined in future works.

## Acknowledgements

This paper acknowledges the support of the Natural Sciences & Engineering Research Council of Canada (NSERC) grant #RGPIN-2017-06707.

## References

- [1] M. Zhang, X. Tao, R. Yu, Y. He, X. Li, X. Chen, W. Huang, Self-healing, mechanically robust, 3D printable ionogel for highly sensitive and long-term reliable ionotronics, *J. Mater. Chem. A* 10 (2022) 12005–12015. doi:10.1039/D1TA09641A.
- [2] C. Fu, K. Wang, W. Tang, A. Nilghaz, C. Hurren, X. Wang, W. Xu, B. Su, Z. Xia, Multi-sensorized pneumatic artificial muscle yarns, *Chemical Engineering Journal* 446 (2022) 137241. doi:10.1016/j.cej.2022.137241.
- [3] W. Qiu, C. Zhang, G. Chen, H. Zhu, Q. Zhang, S. Zhu, Colorimetric ionic organohydrogels mimicking human skin for mechanical stimuli sensing and injury visualization, *ACS Applied Materials & Interfaces* 13 (22) (2021) 26490–26497. doi:10.1021/acsami.1c04911.

- [4] K. D. Harris, A. L. Elias, H.-J. Chung, Flexible electronics under strain: A review of mechanical characterization and durability enhancement strategies, *Journal of Materials Science* 51 (6) (2015) 2771–2805. doi:10.1007/s10853-015-9643-3.
- [5] Y. Liu, L. Wang, Y. Mi, S. Zhao, S. Qi, M. Sun, B. Peng, Q. Xu, Y. Niu, Y. Zhou, Transparent stretchable hydrogel sensors: materials, design and applications, *J. Mater. Chem. C* 10 (2022) 13351–13371. doi:10.1039/D2TC01104B.
- [6] X. Li, Z. Liu, Y. Liang, L.-M. Wang, Y. D. Liu, Chitosan-based double cross-linked ionic hydrogels as a strain and pressure sensor with broad strain-range and high sensitivity, *J. Mater. Chem. B* 10 (2022) 3434–3443. doi:10.1039/D2TB00329E.
- [7] B. Yang, W. Yuan, Highly stretchable, adhesive, and mechanical zwitterionic nanocomposite hydrogel biomimetic skin, *ACS Applied Materials & Interfaces* 11 (43) (2019) 40620–40628, PMID: 31595740. doi:10.1021/acsami.9b14040.
- [8] C. Zhao, Y. Wang, G. Tang, J. Ru, Z. Zhu, B. Li, C. F. Guo, L. Li, D. Zhu, Ionic flexible sensors: Mechanisms, materials, structures, and applications, *Advanced Functional Materials* 32 (17) (2022) 2110417. doi:10.1002/adfm.202110417.
- [9] L.-Y. Zhou, J. Fu, Y. He, A review of 3D printing technologies for soft polymer materials, *Advanced Functional Materials* 30 (28) (2020) 2000187. doi:10.1002/adfm.202000187.
- [10] H. Wang, B. Zhang, J. Zhang, X. He, F. Liu, J. Cui, Z. Lu, G. Hu, J. Yang, Z. Zhou, R. Wang, X. Hou, L. Ma, P. Ren, Q. Ge, P. Li, W. Huang, General one-pot method for preparing highly water-soluble and biocompatible photoinitiators for digital light processing-based 3d printing of hydrogels, *ACS Applied Materials & Interfaces* 13 (46) (2021) 55507–55516, PMID: 34767336. doi:10.1021/acsami.1c15636.
- [11] Y. Rioux, J. Fradette, Y. Maciel, A. Bégin-Drolet, J. Ruel, Biofabrication of sodium alginate hydrogel scaffolds for heart valve tissue engineering, *International Journal of Molecular Sciences* 23 (15) (2022). doi:10.3390/ijms23158567.
- [12] B. Ying, X. Liu, Skin-like hydrogel devices for wearable sensing, soft robotics and beyond, *iScience* 24 (11) (2021) 103174. doi:10.1016/j.isci.2021.103174.
- [13] C. W. Beh, D. S. Yew, R. J. Chai, S. Y. Chin, Y. Seow, S. S. Hoon, A fluid-supported 3d hydrogel bioprinting method, *Biomaterials* 276 (2021) 121034. doi:10.1016/j.biomaterials.2021.121034.
- [14] C. Yang, Z. Suo, Hydrogel ionotronics, *Nature Reviews Materials* 3 (6) (2018) 125–142. doi:10.1038/s41578-018-0018-7.
- [15] A. E. Emerson, A. B. McCall, S. R. Brady, E. M. Slaby, J. D. Weaver, Hydrogel injection molding to generate complex cell encapsulation geometries, *ACS Biomaterials Science & Engineering* 8 (9) (2022) 4002–4013. doi:10.1021/acsbmaterials.2c00640.
- [16] Y. Li, J. D. Motschman, S. T. Kelly, B. B. Yellen, Injection molded microfluidics for establishing high-density single cell arrays in an open hydrogel format, *Analytical Chemistry* 92 (3) (2020) 2794–2801. doi:10.1021/acs.analchem.9b05099.
- [17] J.-Y. Sun, C. Keplinger, G. M. Whitesides, Z. Suo, Ionic skin, *Advanced Materials* 26 (45) (2014) 7608–7614. doi:10.1002/adma.201403441.
- [18] Y. Wang, P. Chen, X. Zhou, Y. Liu, N. Wang, C. Gao, Highly sensitive zwitterionic hydrogel sensor for motion and pulse detection with water retention, adhesive, antifreezing, and self-healing properties, *ACS Applied Materials & Interfaces* 14 (41) (2022) 47100–47112, PMID: 36194533. doi:10.1021/acsami.2c14157.
- [19] H. Liu, X. Wang, Y. Cao, Y. Yang, Y. Yang, Y. Gao, Z. Ma, J. Wang, W. Wang, D. Wu, Freezing-tolerant, highly sensitive strain and pressure sensors assembled from ionic conductive hydrogels with dynamic cross-links, *ACS Applied Materials & Interfaces* 12 (22) (2020) 25334–25344, PMID: 32422039. doi:10.1021/acsami.0c06067.
- [20] Y. Bai, B. Chen, F. Xiang, J. Zhou, H. Wang, Z. Suo, Transparent hydrogel with enhanced water retention capacity by introducing highly hydratable salt, *Applied Physics Letters* 105 (15) (2014) 151903. doi:10.1063/1.4898189.
- [21] X. Sui, H. Guo, C. Cai, Q. Li, C. Wen, X. Zhang, X. Wang, J. Yang, L. Zhang, Ionic conductive hydrogels with long-lasting antifreezing, water retention and self-regeneration abilities, *Chemical Engineering Journal* 419 (2021) 129478. doi:10.1016/j.cej.2021.129478.
- [22] X. Sui, H. Guo, C. Cai, Q. Li, C. Wen, X. Zhang, X. Wang, J. Yang, L. Zhang, Ionic conductive hydrogels with long-lasting antifreezing, water retention and self-regeneration abilities, *Chemical Engineering Journal* 419 (2021) 129478. doi:10.1016/j.cej.2021.129478.
- [23] H. Bai, D. Chen, H. Zhu, S. Zhang, W. Wang, P. Ma, W. Dong, Photocrosslinking ionic conductive pva-sbq/fec13 hydrogel sensors, *Colloids and Surfaces A: Physicochemical and Engineering Aspects* 648 (2022) 129205. doi:10.1016/j.colsurfa.2022.129205.
- [24] F. Ahmadi, Z. Oveisi, S. Samani, Z. Amoozgar, Chitosan based hydrogels: characteristics and pharmaceutical applications, *Research in Pharmaceutical Sciences* 10 (1) (2015) 1–16.
- [25] S. Wang, Z. Sun, Y. Zhao, L. Zuo, A highly stretchable hydrogel sensor for soft robot multi-modal perception, *Sensors and Actuators A: Physical* 331 (2021) 113006. doi:10.1016/j.sna.2021.113006.
- [26] T. Zhu, C. Jiang, M. Wang, C. Zhu, N. Zhao, J. Xu, Skin-inspired double-hydrophobic-coating encapsulated hydrogels with enhanced water retention capacity, *Advanced Functional Materials* 31 (27) (2021) 2102433. doi:10.1002/adfm.202102433.
- [27] W. Zhao, Z. Lin, X. Wang, Z. Wang, Z. Sun, Mechanically interlocked hydrogel–elastomer strain sensor with robust interface and enhanced water–retention capacity, *Gels* 8 (10) (2022).
- [28] X.-Y. Yin, Y. Zhang, J. Xiao, C. Moorlag, J. Yang, Monolithic dual-material 3d printing of ionic skins with long-term performance stability, *Advanced Functional Materials* 29 (39) (2019) 1904716. doi:10.1002/adfm.201904716.
- [29] Q. Gao, X. Niu, L. Shao, L. Zhou, Z. Lin, A. Sun, J. Fu, Z. Chen, J. Hu, Y. Liu, Y. He, 3d printing of complex gelma-based scaffolds with nanoclay, *Biofabrication* 11 (3) (2019) 035006. doi:10.1088/1758-5090/ab0cf6.
- [30] P. Dorishetty, R. Balu, S. S. Athukoralalage, T. L. Greaves, J. Mata, L. de Campo, N. Saha, A. C. W. Zannettino, N. K. Dutta, N. R. Choudhury, Tunable biomimetic hydrogels from silk fibroin and nanocellulose, *ACS Sustainable Chemistry & Engineering* 8 (6) (2020) 2375–2389. doi:10.1021/acssuschemeng.9b05317.
- [31] A. Xavier Mendes, S. Moraes Silva, C. D. O’Connell, S. Duchi, A. F. Quigley, R. M. I. Kapsa, S. E. Moulton, Enhanced electroactivity, mechanical properties, and printability through the addition of graphene oxide to photo-cross-linkable gelatin methacryloyl hydrogel, *ACS Biomaterials Science & Engineering* 7 (6) (2021) 2279–2295, PMID: 33956434. doi:10.1021/acsbmaterials.0c01734.
- [32] S. Liu, L. Li, Ultrastretchable and self-healing double-network hydrogel for 3d printing and strain sensor, *ACS Applied Materials & Interfaces* 9 (31) (2017) 26429–26437, PMID: 28707465. doi:10.1021/acsami.7b07445.
- [33] M. Janmaleki, J. Liu, M. Kamkar, M. Azarmanesh, U. Sundararaj, A. S. Nezhad, Role of temperature on bio-printability of gelatin methacryloyl bioink in two-step cross-linking strategy for tissue engineering applications, *Biomedical Materials* 16 (1) (2020) 015021. doi:10.1088/1748-605X/abbcc9.
- [34] Y. Zhou, Y. Cui, L.-Q. Wang, A dual-sensitive hydrogel based on poly(lactide-co-glycolide)-polyethylene glycol-poly(lactide-co-glycolide) block copolymers for 3d printing., *International Journal of Bioprinting* 7 (2021). doi:10.18063/ijb.v7i3.389.
- [35] Y. Zhang, L. Chen, M. Xie, Z. Zhan, D. Yang, P. Cheng, H. Duan, Q. Ge, Z. Wang, Ultra-fast programmable human-machine interface enabled by 3d printed degradable conductive hydrogel, *Materials Today Physics* 27 (2022) 100794. doi:10.1016/j.mtphys.2022.100794.
- [36] H. Zhu, X. Hu, B. Liu, Z. Chen, S. Qu, 3d printing of conductive hydrogel–elastomer hybrids for stretchable electronics, *ACS Applied Materials & Interfaces* 13 (2021) 59243. doi:10.1021/acsami.1c17526.
- [37] G. Sennakesavan, M. Mostakhdemin, L. Dkhar, A. Seyfoddin, S. Fathihi, Acrylic acid/acrylamide based hydrogels and its properties - a review, *Polymer degradation and stability* 180 (2020) pp. 109308–. doi:10.1016/j.polymdegradstab.2020.109308.